Numerical Analysis and Experiments of a Microwave-Excited Microplasma Thruster

IEPC-2007-029

Presented at the 30th International Electric Propulsion Conference, Florence, Italy
September 17-20, 2007

Takeshi Takahashi*, Yoshinori Takao†, Koji Eriguchi‡ and Kouichi Ono§
Graduate School of Engineering, Kyoto University, Kyoto, 606-8501, Japan

A microwave-excited plasma source for microthrusters has been investigated numerically and experimentally. The microplasma source consisted of a dielectric chamber, 0.75 mm in radius and 10 mm long, and a metal that covers it. The gas temperature reached 1050 K around the top of the antenna, being in good agreement with the experimental result. This numerical model enabled us to predict the discharge characteristics in the microplasma source and to optimize the configuration.

I. Introduction

In recent years, the trend of space systems has been focused on miniaturization and simplification of the structure, to reduce the mission costs and increase the launch rates. Missions with numerous small-scale satellites, called "nanosatellites", would bring a significant advantage of reducing the mission risk.[1] Such concept has supported a new approach to develop accurate, reliable, and low-cost micropropulsion systems, particularly for high-accuracy station-keeping and attitude control.

In this paper, we report on a microplasma thruster with surface wave-excited plasma (SWP) sources, with emphasis being placed on numerical evaluation of the property of SWP sources by taking into account the spatial distribution of plasma parameters therein. A remarkable feature of SWPs is the electron heating that occurs in a thin skin-depth layer along the plasma-dielectric interfaces;[2] that is, the power absorption in plasmas becomes maximum at the interfaces. This is a great advantage to generate plasmas in a very small space. In effect, the smaller the dimension is, the larger the surface-to-volume ratio is, which leads to a significant diffusion loss to the wall. Another advantage of microwave plasmas is that there is no electrode; thus, a serious lifetime problem caused by plasma sputtering is avoided.

Figure 1 shows a cross-sectional view of the microplasma thruster presently developed, which consists of an azimuthally symmetric surface wave-excited plasma source and a conical micronozzle for exhausting the plasma.[4,5] The microplasma source is composed of a dielectric chamber, 0.75 mm in radius and 10 mm long, and a metal around the chamber.

Microwaves propagate through a coaxial cable which is connected to the left end of the plasma chamber, and then penetrate into the chamber, where the propellant is ionized and heated up by surface waves. The high thermal energy is converted into directional kinetic energy through the nozzle which has a converging and diverging section, to obtain the thrust. We use argon for the propellant.

II. Numerical Model

The numerical model consisted of two modules: an electromagnetic module (EMM) and a plasma fluid module (PFM). Since it is expected that the high frequency perturbation of electromagnetic waves is separated from the ambipolar electric fields governed by relatively slow plasma evolution,[6] a self-consistent solution was obtained by applying the different timescale integration to two modules. The electromagnetic fields of microwaves were traced by the EMM employing the finite-difference time-domain (FDTD) approximation to Maxwell's equations, and the

*Graduate Student, Department of Aeronautics and Astronautics, Email: t-takahashi@aero.mbox.media.kyoto-u.ac.jp
†Graduate Student, Department of Aeronautics and Astronautics
‡Associate Professor, Department of Aeronautics and Astronautics, Email: eriguchi@kuaero.kyoto-u.ac.jp
§Professor, Department of Aeronautics and Astronautics, Email: ono@kuaero.kyoto-u.ac.jp

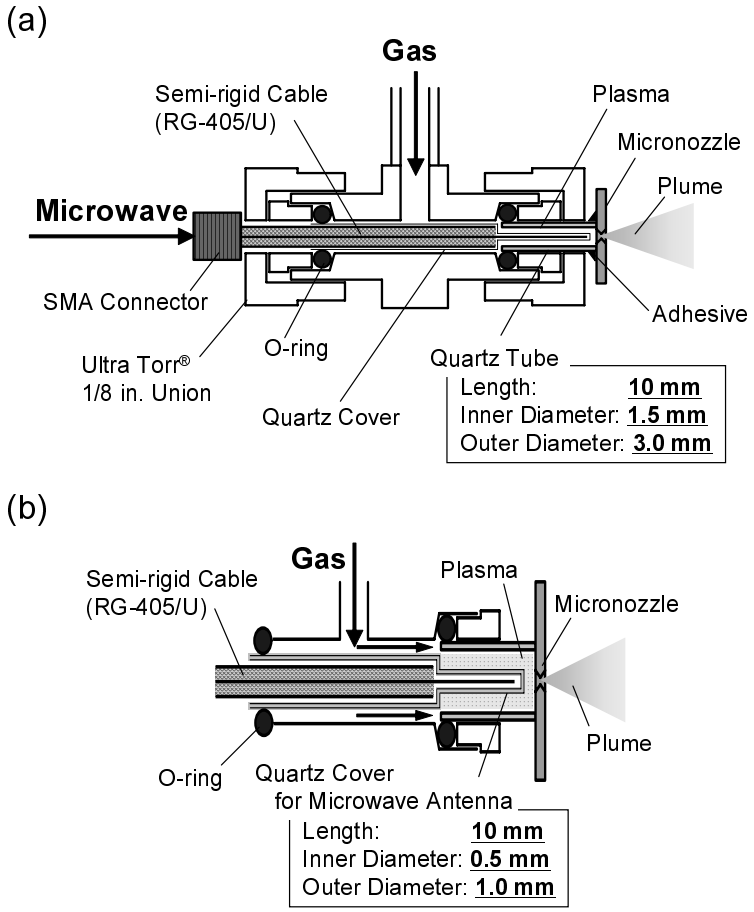

Figure 1. (a) Cross-sectional view of a microplasma thruster, and (b) its radially enlarged view showing the feed of propellant gases.

plasma evolution was traced by the PFM employing an explicit scheme for plasma fluid equations (Fig. 2). The FDTD unit cell and fluid unit cell are shown in Fig. 3 for the cylindrical coordinates.

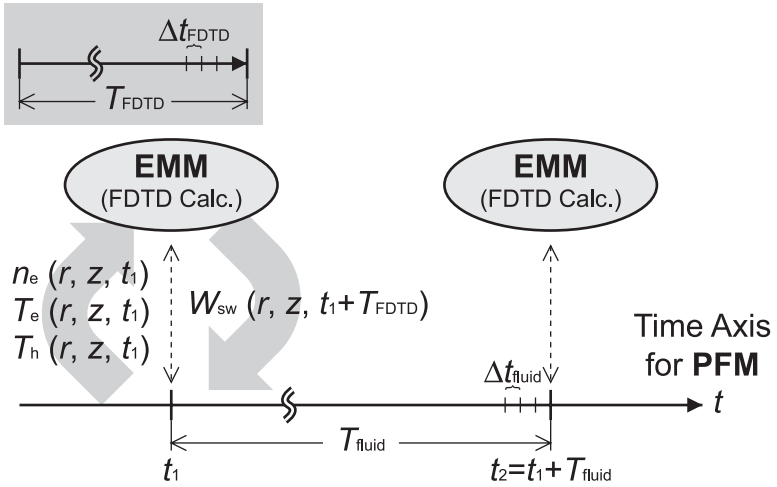

Figure 2. Schematic of the algorithm employed in the simulation.

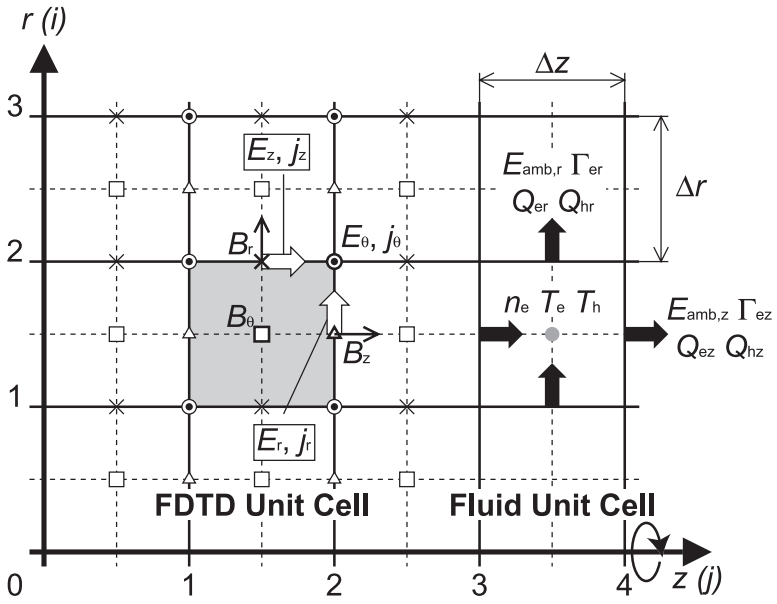

Figure 3. FDTD unit cell and fluid unit cell in the cylindrical coordinates.

III. Numerical Results and Discussion

In the simulation, the time steps for EMM and PFM were taken to be $\Delta t_{FDTD} = 4.0\times10^{-14}$ s and $\Delta t_{fluid} = 3.2\times10^{-13}$ s, respectively. The spatial steps were taken to be $\Delta r = \Delta z = 4.0 \times 10^{-5}$ m. Initially at $t = 0$, the plasma was assumed to have a spatially uniform electron density of $n_e = 1.5 \times 10^{20}$ m^{-3} (larger than the critical density $n_{cr} \approx 9.51 \times 10^{17}$ m^{-3} for the surface-wave propagation at a microwave frequency of 4.0 GHz) and an electron temperature of $kT_e = 2.0$ eV. A steady-state solution for the distribution of n_e, T_e and T_h was obtained within $t = 1.0 - 4.0 \times 10^{-6}$ s. It is further noted that the steady-state solutions depended on gas pressure, microwave frequency, temperature of the chamber wall, and relative permittivity of the chamber. The solution did not depend on the initial distribution of n_e, T_e and T_h, as long as the initial electron density is larger than n_{cr}.

The simulation was performed under the following conditions: background gas pressure $p_n = 20$ kPa, microwave

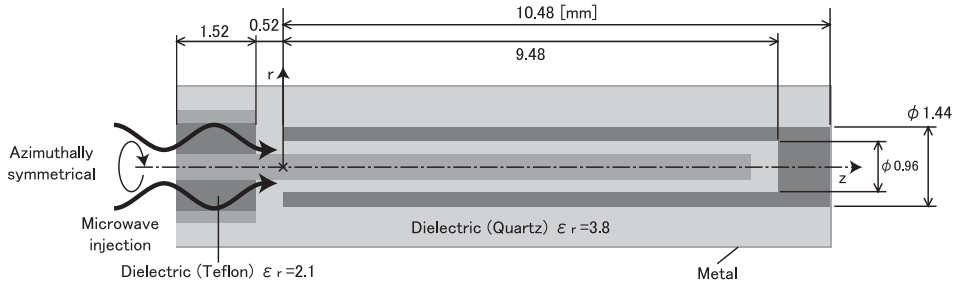

Figure 4. Schematic of the calculation area.

frequency f = 4.0 GHz, temperature of the chamber wall T_w = 500 K, relative permittivity of the chamber ϵ_r = 3.8, and length of the chamber l = 10.48 mm. The total microwave power absorbed by the plasma was P_{abs} = 5.0 W. The two-dimensional distributions of the electron density, absorbed power, electron temperature, and heavy particle temperature are shown in Figs. 5 (a) - 5 (d). The total incident microwave power was P_{in} = 5.2 W at the monitor plane (z = −0.8 mm). The propellant gas was ionized near the top of the antenna (Fig. 5 (a)), and the heavy particle temperature reached 1050 K (Fig. 5 (d)).

Then, in order to investigate the dependence of plasma characteristics on discharge conditions, the simulation was also performed under different conditions as follows: background gas pressure p_n = 10, 20, 50 kPa, microwave frequency f = 4.0, 10 GHz, length of the chamber l = 4.48 − 12.48 mm, and the total absorbed microwave power P_{abs} = 3.0, 5.0, 7.0 W. Figs. 6 (a) and (b) show the electron density n_e and the heavy particle temperature T_h as a function of total absorbed microwave power P_{abs}. The electron density and heavy particle temperature rose with increasing P_{abs}. Under higher pressure (50 kPa), the calculated electron density was 20% lower than the other conditions, because more frequent collision occurred between electrons and neutrals. Figs. 7 (a) and (b) show the electron density n_e and heavy particle temperature T_h as a function of the length of plasma chamber l. When we used 4.0-GHz microwaves, the electron density and heavy particle temperature had little dependence on the plasma length. This leads to an advantage of 4.0-GHz microwaves that the plasma characteristics are little affected by the shape of plasma source. On the other hand, when we used 10-GHz microwaves, higher electron density and heavy particle temperature were achieved with shorter (l = 4.48, 5.48 mm) plasma chamber. This result indicates that 10-GHz microwaves and short chamber can improve thrust performance.

IV. Experiments

The microplasma source for microthrusters was investigated by optical emission spectroscopy (OES) using the N_2 rotational spectrum. Fig. 8 shows photograph images of the Ar plasma jet plume expanding into vacuum through a micronozzle at the end of the microplasma source. The heavy particle temperature was measured by OES, being 700 - 1200 K near the nozzle inlet (Fig. 9). Also, the heavy particle temperature increased with increasing incident microwave power P_{in}.

We also investigated the plasma source by OES using the H-Balmer-β spectrum, to obtain the electron density therein.[7] The obtained spectrum and the numerical fit by Voigt profile are shown in Fig. 10. The Voigt profile can be deconvolved into Gaussian component and Lorenzian component, and the latter depends on the electron density because of Stark effect. Thus, the electron density in the plasma source can be calculated by measuring the spectrum width.

Fig. 11 shows the electron density measured by Stark effect and that predicted by numerical analysis. The electron density also increased with increasing P_{abs}.

V. Conclusions

Plasma characteristics of the microplasma source for thrusters have been investigated numerically and experimentally. The electron density and heavy particle temperature obtained by numerical analysis were in good agreement with the experimental results by OES. This numerical method enabled us to predict the discharge characteristics in the microplasma source and to optimize the configuration.

(a) n_e (10^{18} m^{-3})

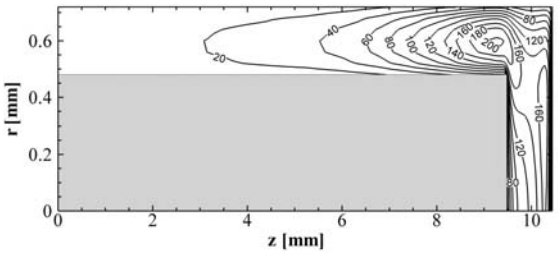

(b) Q_{abs} (10^6 Wm^{-3})

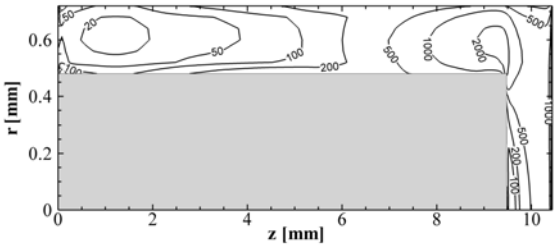

(c) T_e (K)

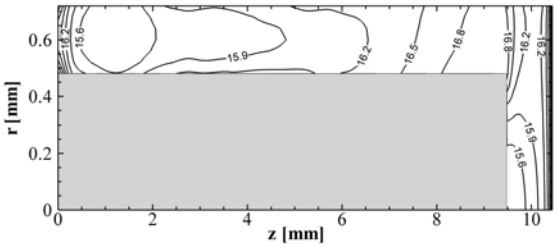

(d) T_h (K)

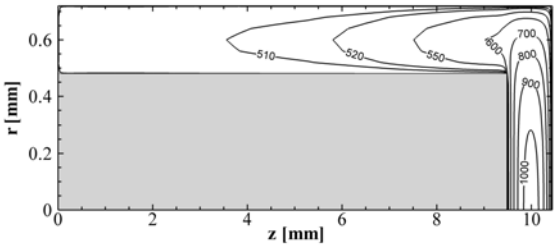

Figure 5. 2D distribution of (a) electron density n_e, (b) absorbed power Q_{abs}, (c) electron temperature T_e, and (d) heavy particle temperature T_h in the microplasma source.

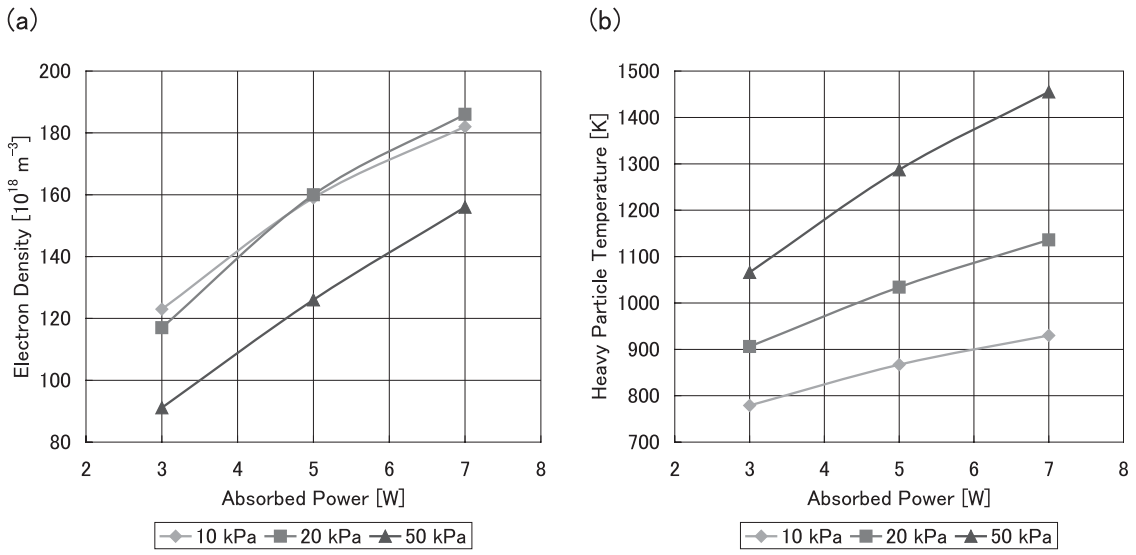

Figure 6. (a) Electron density and (b) heavy particle temperature as a function of microwave power P_{abs}.

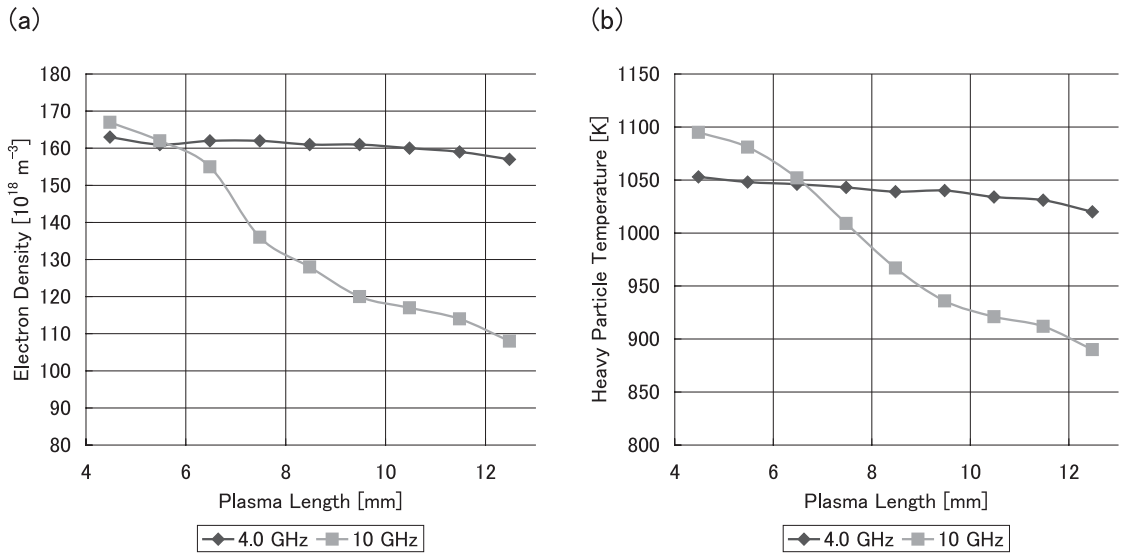

Figure 7. (a) Electron density and (b) heavy particle temperature as a function of length of plasma source.

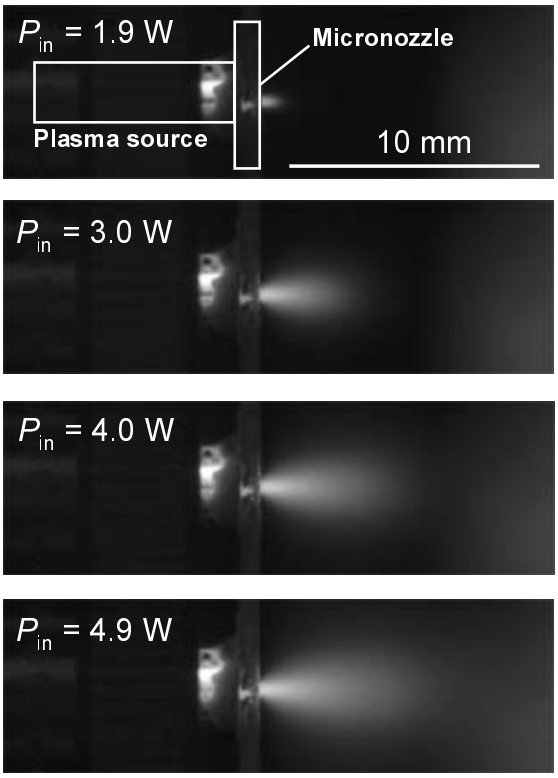

Figure 8. Photograph images of the Ar plasma jet plume expanding into vacuum through a micronozzle at the end of the microplasma source.

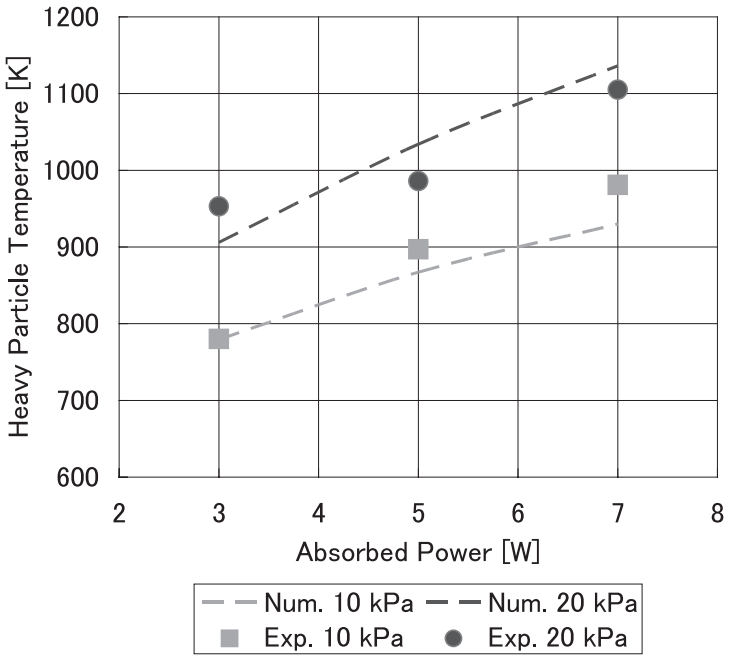

Figure 9. N_2 rotational temperature as a function of absorbed microwave power P_{abs}.

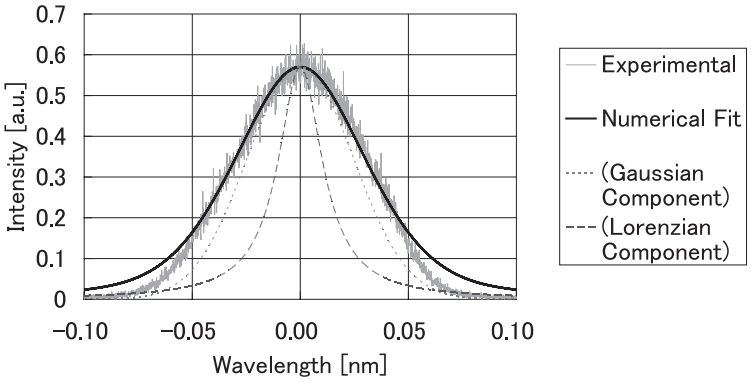

Figure 10. Observed H-Balmer-β spectrum and the numerical fit.

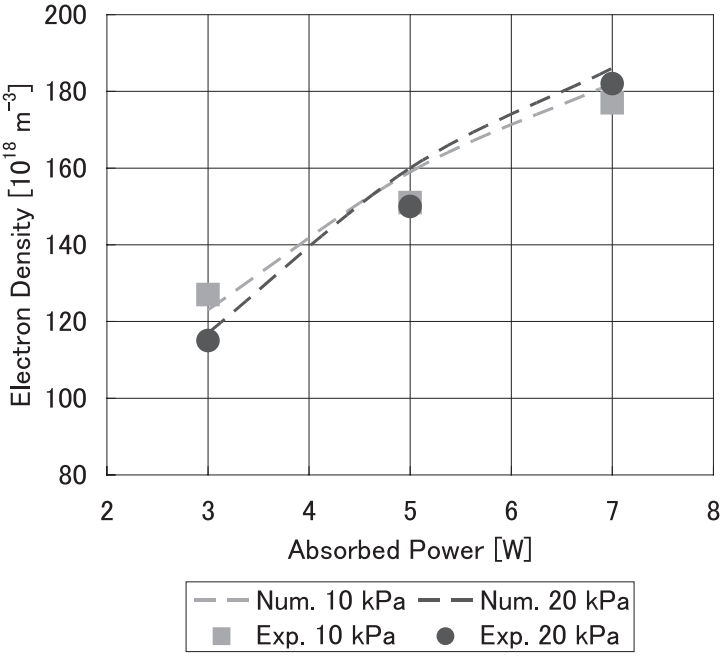

Figure 11. Electron density as a function of absorbed microwave power P_{abs}.

References

[1]J. Mueller: AIAA 97-3058.
[2]I. Ganachev and H. Sugai: Surface and Coating Technology. **174-175** (2003) 15.
[3]H. Kousaka and K. Ono: Jpn. J. Appl. Phys. **41** (2002) 2199.
[4]Y. Takao and K. Ono: Plasma Sources Sci. Technol. **15** (2006) 211.
[5]Y. Takao, K. Ono, K. Takahashi, and K. Eriguchi: Jpn. J. Appl. Phys. **45** (2006) 8235.
[6]H. Kousaka and K. Ono: Plasma Sources Sci. Technol. **12** (2003) 273.
[7]Q. Wang, I. Koleva, V. M. Donnelly and D. J. Economou: J. Phys. D: Appl. Phys. **38** (2005) 1690.
[8]R. A. Stewart, P. Vitello, D. B. Graves, E. F. Jaeger and L. A. Berry: Plasma Sources Sci. Technol. **4** (1995) 36.
[9]E. W. McDaniel, J. B. A. Mitchell and M. E. Rudd: *Atomic Collisions: Heavy Particle Projectiles* (Wiley, 1993, New York).
[10]M. A. Lieberman and A. J. Lichtenberg: *Principles of Plasma Discharges and Materials Processing (2nd Edition)* (Wiley, 2005, New York).